Improved Shear Wave-front Reconstruction Method by Aligning Imaging Beam Angles with Shear-wave Polarization: Applied for Shear Compounding Application

Safeer Hyder, Sevan Harput, Zainab Alomari, David M. J. Cowell, James McLaughlan and Steven Freear
Ultrasound Group, School of Electronic and Electrical Engineering, University of Leeds, UK.
Email: el10shl@leeds.ac.uk

***Abstract*—In shear compounding, shear waves are generated at various angles and individual elasticity maps are averaged to reduce noise and improve accuracy. The steered shear waves tilt the tissue motion direction therefore conventional plane wave tracking is not capable of capturing true shear wave amplitude and direction. The proposed method aligns the tracking beams with the shear wave angles, enables beam-axis in the direction of tissue motion to estimate true shear wave motion vector. In this experimental work, shear waves are produced at five different angles and motion is captured using proposed and conventional method. All the experiments are conducted using inclusion-based elasticity phantom. In the results, the displacement maps show that proposed method accurately captured the steered push-beam wave-fronts while conventional method produced push-beam direction artefacts. In the final compounded elasticity maps, the proposed method slightly improved background-to-inclusion elasticity ratio, CNR by 2 dB, and produced inclusion boundary shape sharper than the conventional tracking.**

I. Introduction

Elastic properties of the soft tissues have been used as biomarker for diagnosis and staging various diseases such as liver fibrosis staging [1], [2], breast lesion [3], and thyroid nodule differential diagnosis [4]. The ultrasound shear wave elastography is able to produce 2-D elasticity maps of soft tissues within few milli-seconds, which is based on generation and calculation of shear wave propagation speed in the medium. Assuming the tissue is linear, incompressible, isotropic, and purely elastic, shear wave speed (c_s) is related with Young's modulus (μ) using following expression, where ρ is the mass density of the medium [5]

$$\mu = \rho c_s^2 \tag{1}$$

Two commercially available shear wave elastography techniques are supersonic shear-wave imaging (SSI) [5] and comb-push ultrasound shear-wave elastography (CUSE) [6]. To enhance the stiffness estimation accuracy, the spatial shear compounding technique was proposed for both SSI and CUSE [5], [7]. In B-mode imaging, spatial compounding techniques are widely used to improve B-mode image quality and speckle tracking [8], [9]. In the shear compounding, similar phenomenon is used and shear wave fields are produced from various directions and individual elasticity maps are averaged to minimize random noise and to improve inclusion geometry reconstruction [5], [7]. In SSI, shear compounding was achieved using supersonic phenomenon, and tilted shear waves were induced at different angles using different Mach numbers [5]. While, Song et al. exploited various sub-apertures of the curvilinear array to produce differently angled shear waves [7]. When zero angle shear waves are generated, waves propagate laterally while corresponding motion vector is orthogonal to the propagation direction (axial direction), and eventually aligned with the imaging beam-axis. The challenge arises when steered shear waves are generated and it changes the direction of motion vector as well, creating both axial and lateral components of the motion. To estimate the angled motion vector, there were various methods proposed in the research for both blood-flow and elastography applications. The strain elastography also share the similar challenge [10], and to overcome this limitation, U. Techavipoo, et al. presented a method to measure both axial and lateral tissue motion by curve fitting angular displacements from multi-angle insonifications [6]. Another method proposed by the Tanter, et al. used two differently angled insonifications from separate sub-apertures of the array, and estimated 2-D displacement tissue motion [9].

In this study, we propose a method in which tracking beam (insonification) angles are adjusted to push-beam angles (shear wave beam) so that tissue motion is aligned with acoustic beam axis. The method is applied for five different push-beam angles. In conventional shear elastography, three angles are used to improve speckle tracking accuracy SNR [8] and the central angle is always zero while other two are selected by adding and subtracting 2 or 4 from the central angle [9]. Using proposed technique, three compounding angles for displacement estimation are used while central angle is parallel to the push-beam angle and other two angles are calculated by adding and subtracting 2 from the push-beam angle, as shown in Fig. 1. For this paper, aligned tracking terminology is used for the proposed method while conventional tracking for fixed shear wave tracking beams. The proposed method was used to image a commercially available elasticity phantom and the results were compared with the conventional tracking

method in terms of background-to-inclusion ratio (BIR), and CNR (contrast-noise-ratio).

II. Materials and Methods

Ultrasound array research platform II (UARPII), developed by Ultrasound Group, University of Leeds was used for the RF data acquisition [11], [12]. The 128 element L3-8/40EP (Prosonic Co., Ltd, Korea) medical probe with centre frequency of 4.79 MHz was used for shear wave generation and tracking. Five push-beam angles were tested for both aligned and conventional tracking schemes and are listed as (-15°, -10°, 0°, +10°, +15°). For shear wave generation, three focused (focal depth 30 mm) push-beams, 16 elements each were used, with tone burst of 570 μs. After shear wave generation, for aligned tracking scheme, the corresponding imaging compounding angles used were (-17°, -15°, -13°), (-12°, -10°, -8°) , (-2°, 0° +2°) , (+12°, +10°, +8°) , and (+17°, +15°, +13°), for (-15°, -10°, 0° , +10° , +15°) push-beam angles, respectively. In conventional tracking scheme, compounding angles were fixed to (-2°, 0°, +2°) for all the push-beam angles.

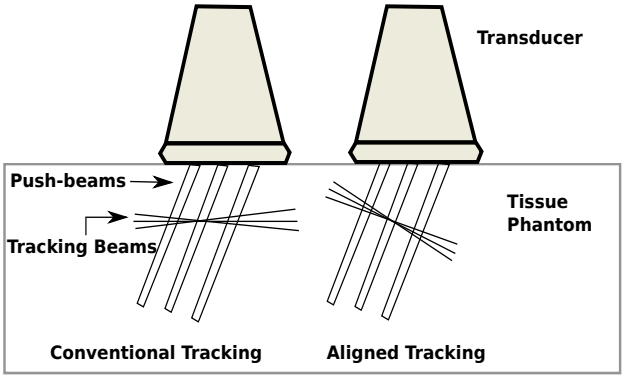

Fig. 1. The schematic diagram of the aligned and conventional shear wave tracking. In aligned tracking beams, three imaging beams are placed around push-beam angle while in conventional tracking imaging beams are placed around zero degree.

The RF data was beamformed using classical delay-and-sum beamformer [8], [14]. After shear wave generation, motion data was acquired at frame-rate of 10 kHz, with effective frame-rate of 3.33 kHz after averaging three multiple-angle B-mode images. For shear wave motion estimation, 1-D normalized cross-correlation was performed, with kernel length of 2 mm ($\sim 6\lambda$) and step of 0.304 mm ($\sim \lambda$). To separate complex shear wave field into left and right travelling shear waves, directional filtering was performed [6]. For shear wave speed estimation, a 2-D shear wave speed estimation algorithm was applied with kernel size of 2.4 mm and patch size of 1.2 mm in the lateral and axial direction, as proposed by the [7]. The duration of shear wave generation and data acquisition was 15 ms. For final elasticity maps, no smoothing filter was used.

For elasticity imaging purpose, a multi-purpose, multi-tissue ultrasound phantom (CIRS., Norfolk, VA) was used, with

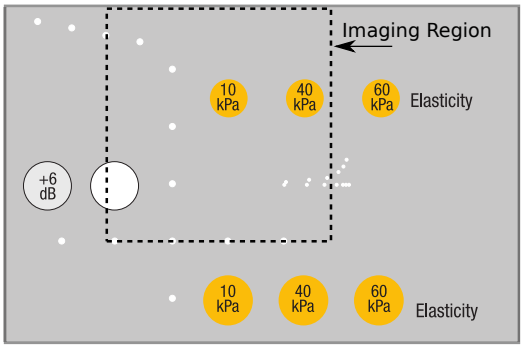

Fig. 2. The schematic diagram of the CIRS phantom and imaging region. The imaging region consist of 40 mm in the axial and 50 mm in the lateral direction.

acoustic speed of 1540 m/s, attenuation of 0.5 dB/cm/MHz and density of 1050 kg/m^3. The 6 mm cylindrical inclusion is centred at 15 mm from surface of the transducer. The Young's modulus of the inclusion is 10±3 kPa, and background has a Young's modulus of 22±5 kPa, while stiffness of the background is 2.2 times greater than the inclusion. The acoustic and mechanical parameters of the phantom are tested and provided by the manufacturer. For performance comparison, the background-to-inclusion ratio and contrast-to-noise ratio in dB were calculated for Young's modulus values, and a 5 x 5 mm rectangular region-of-interest (ROI) inside the inclusion, and two ROI surrounding the inclusion were used for these calculations. The following expression was used for CNR, where C_I and C_B are mean Young's modulus values in the inclusion and background, respectively; while σ_B is standard deviation of the Young's modulus of the background [6]

$$\text{CNR} = 20\log_{10}\left[\frac{|C_I - C_B|}{\sigma_B}\right] \tag{2}$$

III. Results and Discussion

This study shows a difference in the shear wave motion tracking accuracy, when tracking beams are aligned with the push-beam angles, in contrast to conventional tracking schemes. When tracking beams are on the same axis as tissue motion, true angle of the shear wave-front is reconstructed and displacement SNR is improved, and final compounded elasticity maps improved the inclusion boundary reconstruction, CNR and elasticity ratio between inclusion and background.

The shear wave displacement maps for all experiments are produced at 0.1 ms after shear wave generation is ceased, and presented in the Fig. 3. In the conventional tracking maps (Figs. 3a, 3b, 3c, 3d), it can be observed that conventional tracking angles produced artefacts (pointed by the arrows) which falsely reconstructs the direction of the push-beam angle as zero-angle push-beam, while true push-beam angles are (-15°, -10°, +10°, +15°). When tracking beams were switched to aligned tracking (Figs. 3f, 3g, 3h, 3i), the artefacts are fully suppressed and true push-beam direction is estimated, while there is no overlapping between two push-beams.

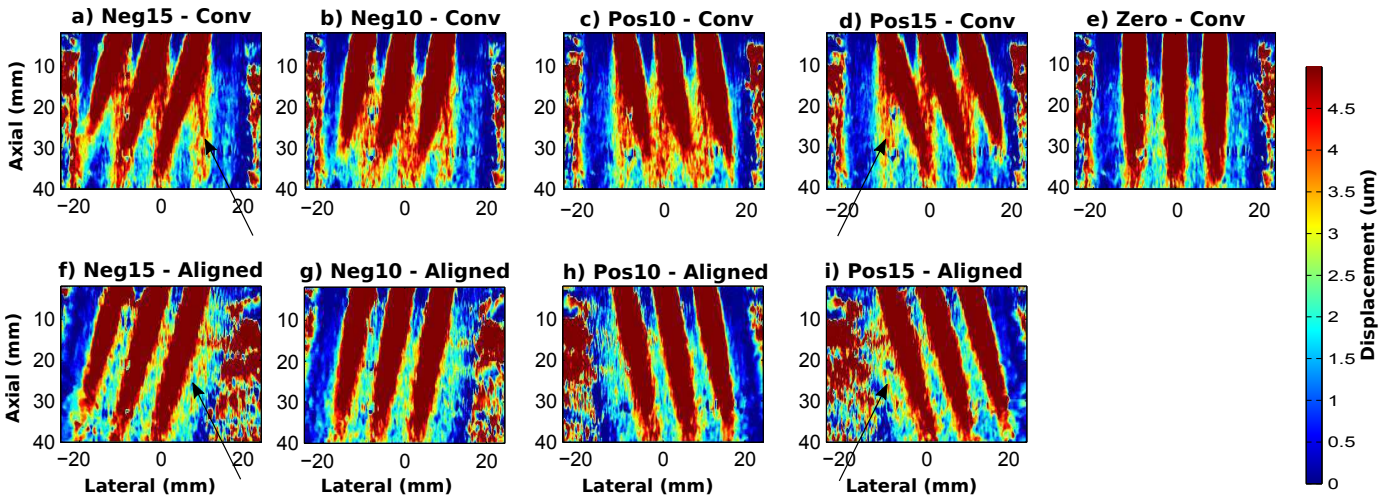

Fig. 3. The displacement maps for aligned and conventional tracking beams used for listed (-15°, -10°, 0°, +10°, +15°) push-beam angles at time instant of 0.1 ms after ultrasound switches to imaging mode. The labels on each displacement map indicate the push-beam and associated tracking angle. All conventional tracking beams are fixed to (-2°, 0°, +2°), while aligned tracking beams are adjusted to the push-beam angle. The colorbar scale is in the units of μm. The false push-beam angle direction artefact are produced by the conventional tracked maps pointed by arrows (map a and d) while in aligned tracked maps, the push-beam wave-front angle are truly reconstructed (map f and i).

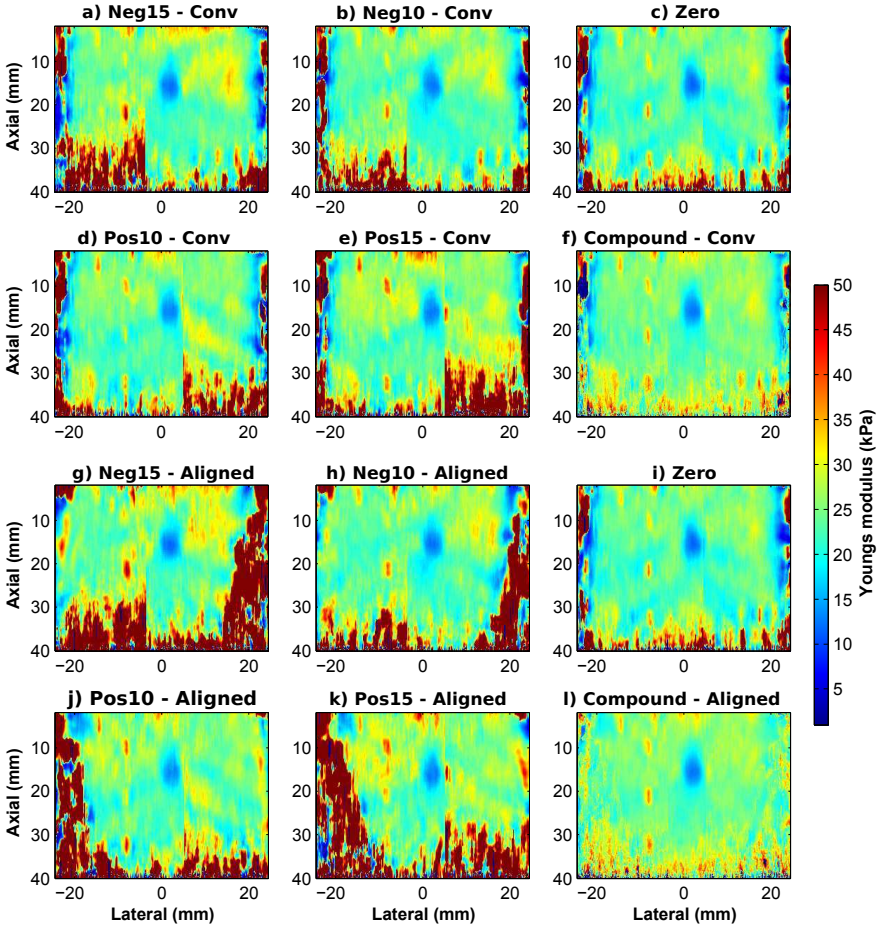

Fig. 4. The Elasticity maps for five push-beam angles and corresponding compounded maps for aligned and conventional tracking methods. The colorbar scale is in units of Young's modulus (kPa).The compounded aligned tracking map (map l) shows improved inclusion geometry, better contrast and higher field-of-view as compared to the conventional tracked compounded map (map f).

TABLE I
YOUNG'S MODULUS BIR AND CNR MEASUREMENTS OF BACKGROUND AND INCLUSION FROM ROI

	Conventional		Aligned	
Push-beam Angle	**BIR**	**CNR (dB)**	**BIR**	**CNR (dB)**
- 15°	1.66	25.87	1.81	22.98
- 10°	1.54	25.18	1.62	25.15
0°	1.50	22.97	1.50	22.97
+ 10°	1.44	23.77	1.40	24.92
+ 15°	1.69	28.54	1.63	23.50
Compounded	1.56	29.05	1.59	31.00

In the zero shear wave angle, there are no artefacts as shear wave and tracking angles are aligned (Fig. 3e). The Young's modulus maps are produced for all the experiments and presented in the Fig. 4. In elasticity measurements, -15° and -10° aligned tracked shear wave maps (Figs. 4g, 4h) have produced sharper inclusion geometry contrast to conventional tracked maps (Figs. 4a, 4b), while in +15° and +10° maps (Figs. 4d, 4e, 4j, 4k), no difference was observed and results are comparable. A zero push-angle maps are same for both aligned and conventional tracking (Fig. 4c). In the final compounded elasticity maps, aligned tracking (Fig. 4l) have preserved inclusion geometry shape better than the conventional tracking (Fig. 4f). In the final compounded maps, the CNR is 2 dB higher for proposed method than the conventional method, and BIR is also slightly improved in the aligned tracked maps (Table I). Performance metrics indicate that, improvement in the shear wave motion tracking is slightly translated to improve the contrast and elasticity estimation accuracy. The improvement could be further achieved if higher shear wave angles were used but using linear arrays, higher steering angles result in widened beamwidth, reduced sensitivity, and grating lobes artefacts, therefore higher steering angles may not improve the results [15]. Furthermore, using proposed technique, elasticity values are achieved in the wider field-of-view (FOV) that is 45 mm as compared to the conventional tracking that is 39 mm. The widened FOV provides elasticity information over the larger area, and it is an additional advantage of the proposed scheme. Ideally, shear compounding requires waves from all directions, but clinically it is not possible. The shear compounding angles can be further increased if mechanical sources are used for shear wave generation as used by Zhao et al. [16].

IV. CONCLUSIONS

In this experimental work, the effect of spatially aligning tracking beams with shear wave polarization is investigated and compared with the conventional method. The results conclude that, angled displacement values are estimated with correct push-beam wave-front while conventional tracking produced artefacts. In the final elasticity maps, aligned tracking improved inclusion contrast and geometry. The results suggest that, spatially aligning shear wave tracking and generation beams improve the motion tracking.

V. ACKNOWLEDGEMENT

The author Safeer Hyder, acknowledges contribution of Sukkur IBA and Higher education commission, Pakistan for supporting his PhD.

REFERENCES

[1] M. Ziol, A. Handra-Luca, A. Kettaneh, C. Christidis, F. Mal, F. Kazemi, V. de Lédinghen, P. Marcellin, D. Dhumeaux, J.-C. Trinchet *et al.*, "Noninvasive assessment of liver fibrosis by measurement of stiffness in patients with chronic hepatitis c," *Hepatology*, vol. 41, no. 1, pp. 48–54, 2005.

[2] G. Ferraioli, C. Tinelli, B. Dal Bello, M. Zicchetti, G. Filice, and C. Filice, "Accuracy of real-time shear wave elastography for assessing liver fibrosis in chronic hepatitis c: A pilot study," *Hepatology*, vol. 56, no. 6, pp. 2125–2133, 2012.

[3] W. A. Berg, D. O. Cosgrove, C. J. Doré, F. K. Schäfer, W. E. Svensson, R. J. Hooley, R. Ohlinger, E. B. Mendelson, C. Balu-Maestro, M. Locatelli *et al.*, "Shear-wave elastography improves the specificity of breast us: the be1 multinational study of 939 masses," *Radiology*, vol. 262, no. 2, pp. 435–449, 2012.

[4] K. S. Bhatia, C. S. Tong, C. C. Cho, E. H. Yuen, Y. Y. Lee, and A. T. Ahuja, "Shear wave elastography of thyroid nodules in routine clinical practice: preliminary observations and utility for detecting malignancy," *European radiology*, vol. 22, no. 11, pp. 2397–2406, 2012.

[5] J. Bercoff, M. Tanter, and M. Fink, "Supersonic shear imaging: a new technique for soft tissue elasticity mapping," *IEEE transactions on ultrasonics, ferroelectrics, and frequency control*, vol. 51, no. 4, pp. 396–409, 2004.

[6] P. Song, H. Zhao, A. Manduca, M. W. Urban, J. F. Greenleaf, and S. Chen, "Comb-push ultrasound shear elastography (cuse): a novel method for two-dimensional shear elasticity imaging of soft tissues," *IEEE transactions on medical imaging*, vol. 31, no. 9, pp. 1821–1832, 2012.

[7] P. Song, A. Manduca, H. Zhao, M. W. Urban, J. F. Greenleaf, and S. Chen, "Fast shear compounding using robust 2-d shear wave speed calculation and multi-directional filtering," *Ultrasound in medicine & biology*, vol. 40, no. 6, pp. 1343–1355, 2014.

[8] G. Montaldo, M. Tanter, J. Bercoff, N. Benech, and M. Fink, "Coherent plane-wave compounding for very high frame rate ultrasonography and transient elastography," *IEEE transactions on ultrasonics, ferroelectrics, and frequency control*, vol. 56, no. 3, pp. 489–506, 2009.

[9] M. Tanter, J. Bercoff, L. Sandrin, and M. Fink, "Ultrafast compound imaging for 2-d motion vector estimation: application to transient elastography," *IEEE transactions on ultrasonics, ferroelectrics, and frequency control*, vol. 49, no. 10, pp. 1363–1374, 2002.

[10] S. Hyder, S. Harput, Z. Alomari, and S. Freear, "Two-way quality assessment approach for tumour detection using free-hand strain imaging," in *2014 IEEE International Ultrasonics Symposium*. IEEE, 2014, pp. 1853–1856.

[11] P. R. Smith, D. M. Cowell, B. Raiton, C. V. Ky, and S. Freear, "Ultrasound array transmitter architecture with high timing resolution using embedded phase-locked loops," *IEEE transactions on ultrasonics, ferroelectrics, and frequency control*, vol. 59, no. 1, pp. 40–49, 2012.

[12] P. R. Smith, D. M. Cowell, and S. Freear, "Width-modulated square-wave pulses for ultrasound applications," *IEEE transactions on ultrasonics, ferroelectrics, and frequency control*, vol. 60, no. 11, pp. 2244–2256, 2013.

[13] Z. Alomari, S. Harput, S. Hyder, and S. Freear, "Selecting the number and values of the cpwi steering angles and the effect of that on imaging quality," in *2014 IEEE International Ultrasonics Symposium*. IEEE, 2014, pp. 1191–1194.

[14] ——, "The effect of the transducer parameters on spatial resolution in plane-wave imaging," in *Ultrasonics Symposium (IUS), 2015 IEEE International*. IEEE, 2015, pp. 1–4.

[15] P. R. Hoskins, K. Martin, and A. Thrush, *Diagnostic ultrasound: physics and equipment*. Cambridge University Press, 2010.

[16] H. Zhao, P. Song, D. D. Meixner, R. R. Kinnick, M. R. Callstrom, W. Sanchez, M. W. Urban, A. Manduca, J. F. Greenleaf, and S. Chen, "External vibration multi-directional ultrasound shearwave elastography (evmuse): Application in liver fibrosis staging," *IEEE transactions on medical imaging*, vol. 33, no. 11, pp. 2140–2148, 2014.